JOURNAL OF PROPULSION AND POWER
Vol. 26, No. 3, May–June 2010

Linear Response of Laminar Premixed Flames to Flow Oscillations: Unsteady Stretch Effects

Preetham*
GE Global Research, Niskayuna, New York 12309
and
Sai K. Thumuluru,† H. Santosh,‡ and Tim Lieuwen§
Georgia Institute of Technology, Atlanta, Georgia 30332-0150

DOI: 10.2514/1.41559

This paper describes the linear response of a laminar premixed flame to harmonic velocity disturbances. It generalizes previous studies by considering the influence of unsteady stretch effects, manifested as variations in the local burning velocity along the wrinkled flame front. Results are derived from analytical solutions of the *G* equation and used to interpret the relative impact of unsteady curvature and hydrodynamic strain. It is shown that the overall linear flame response depends upon two Strouhal numbers, St_2 and St_c, related to the amount of time taken for a flow (St_c) and flame front (St_2) disturbance to propagate the flame length, normalized by the acoustic period. Stretch effects are shown to be characterized by two frequency-dependent Markstein numbers, σ_c^* and σ_s^*, for curvature and hydrodynamic strain, respectively. Unsteady curvature effects on the flame surface area become significant when $|\sigma_c^*|St_2^2 \sim \mathcal{O}(1)$ and are responsible for the experimentally observed reduction in the flame front wrinkle size in the flow direction [referred to as "filtering" by Bourehla and Baillot (Bourehla, A., and Baillot, F., "Appearance and Stability of a Laminar Conical Premixed Flame Subjected to an Acoustic Perturbation," *Combustion and Flame*, Vol. 1143–4, 1998, pp. 303–318.doi:10.1016/S0010-2180(97)00323-4)].

Nomenclature

A	=	instantaneous flame area
G	=	heat release–velocity transfer function
K	=	velocity ratio, $\tilde{\bar{u}}/\tilde{u}_c$
k	=	convective wave number, $\omega_o/\tilde{u}_c$
L_f	=	steady-state flame length
Le	=	Lewis number
le	=	scaled Lewis number, $Ze(1-1/Le)$
M_a	=	Markstein length
$\hat{M}_{a,c}, \hat{M}_{a,s}$	=	Markstein transfer functions, defined in Eq. (6)
Q	=	instantaneous heat release
R	=	burner radius
r	=	instantaneous radial location
S_L	=	laminar burning velocity
St	=	Strouhal number, $\omega_o L_f/\tilde{\bar{u}}$
St_c	=	convective Strouhal number, defined in Eq. (37)
St_2	=	reduced Strouhal number, defined in Eq. (34)
t	=	time
u	=	instantaneous axial velocity
u_c	=	disturbance propagation velocity
v	=	instantaneous radial velocity
Ze	=	Zeldovich number
α	=	flame angle parameter, defined in Eq. (23)
β	=	flame aspect ratio, L_f/R.
ε	=	fluctuating (axial) velocity amplitude, defined in Eq. (16)
ζ	=	instantaneous flame position
ζ_o, ζ_1, ζ'	=	functions, defined in Eq. (17)
η	=	convection velocity parameter, $K\alpha$.
$\hat{\sigma}_c, \hat{\sigma}_s$	=	transfer function for curvature and strain, $\left(\frac{\hat{M}_{a,c}}{R}, \frac{\hat{M}_{a,s}}{R}\right)$
$\sigma_c^*, \sigma_s^*, \sigma^*$	=	parameters, defined in Eqs. (24), (25), and (40).
ω_0	=	excitation frequency

Superscripts

$\bar{}$	=	time average
$'$	=	fluctuation
$\sim$	=	dimensional value of r, t, u, v, and ζ.

I. Introduction

THIS paper investigates the impact of unsteady stretch effects on the linear response of premixed flames to harmonic velocity disturbances. The primary objective of this work is to predict the heat release response of premixed flames to harmonic flow disturbances, motivated by the problem of combustion instabilities [1–4]. These oscillations are destructive to hardware and adversely affect performance and part life.

This problem has been considered in a number of recent investigations [5–8] that have considered effects of frequency, flame shape, and flow disturbance characteristics upon the linear and nonlinear flame response. The key contribution of this paper is introducing the additional affect of unsteady flame stretch on the linear heat release dynamics; analytical models developed to date have largely assumed a flame speed that is independent of stretch. Because acoustic forcing introduces flame wrinkles (e.g., see Fig. 1) for which length inversely scales with disturbance frequency, it can be anticipated that stretch-induced flame speed variations will become significant at high frequencies.

The response of flat premixed flames to unsteady stretch has been considered in several previous studies. Saitoh and Otsuka [9] performed an experimental study of the response of counterflow ethylene air flames to unsteady strain. They observed that the amplitude of the flame position fluctuations decreased with an increase in oscillation frequency. They also noted that the phase lag

Presented as Paper 176 at the 45th AIAA Aerospace Sciences Meeting and Exhibit, Reno, NV, 8 January–8 November 2007; received 10 October 2008; revision received 20 January 2010; accepted for publication 23 January 2010.

*Scientist.
†Graduate Research Assistant, School of Aerospace Engineering.
‡Graduate Research Assistant, School of Aerospace Engineering.
§Associate Professor, School of Aerospace Engineering; tim.lieuwen@aerospace.gatech.edu (Corresponding Author).

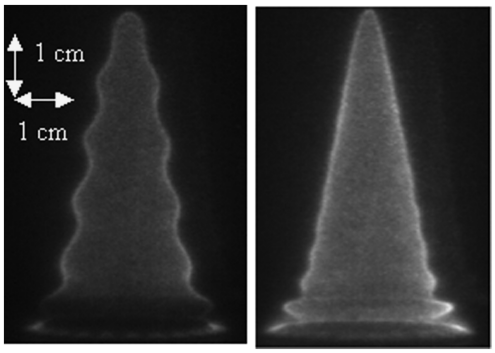

a) b)

Fig. 1 Visualization of an acoustically excited propane flame (equivalence ratio = 0.7, $\tilde{\bar{u}} = 0.8$ m/s, $\tilde{u}'/\tilde{\bar{u}} = 0.2$): a) 100 Hz, and b) 190 Hz. Flow direction is upward.

between the flame position and the incoming flow reached 90 deg at high frequencies. Qualitative agreement with the above conclusions has been obtained in theoretical [10,11] and numerical investigations [12] of the response of premixed flames to oscillating strain rates. Joulin [13] performed a theoretical analysis of the combined effect of unsteady curvature and hydrodynamic strain on the flame propagation speed. It was shown that the stretch sensitivity, characterized by the Markstein length, should be interpreted as integral operators with timewise memory kernels acting on curvature and hydrodynamic strain components. They show that the flame speed dynamically responds to unsteady curvature for all perturbation frequencies. However, the flame speed becomes independent of hydrodynamic strain fluctuations at high frequencies. These predictions were supported by the variable density analysis of Clavin and Joulin [14]. The diminishing sensitivity of flame propagation speed to unsteady strain at high frequencies was also observed by Im and Chen [15], who numerically investigated unsteady strain effects on the burning velocity of hydrogen–air premixed flames in an opposed nozzle configuration. In addition, an analysis of stretch effects on the flame transfer function, similar to that reported in this paper, was also independently performed by Wang [16].

The inclusion of stretch effects in this study is motivated by the observations of Bourehla and Baillot [17], Baillot et al. [18], and Durox et al. [19]. They performed a systematic experimental and theoretical study of the response of a laminar Bunsen (methane) flame to velocity perturbations of varying amplitude and frequency. They found that, at low frequencies ($f < 200$ Hz) and velocity amplitudes ($\tilde{u}'/\tilde{\bar{u}} < 0.3$), the flame front wrinkles symmetrically about the burner axis due to a convected wave traveling from the burner base to its tip. At higher frequencies, but similar low amplitudes, they observed a phenomenon that they refer to as "filtering," wherein the flame wrinkles are only evident at the flame base and decay with axial location downstream. They did not postulate any mechanisms for this behavior. Unfortunately, they did not publish any photographs of the phenomenon either. Lieuwen and Yang [1] postulated that this behavior could be due to the growing significance of flame speed variations along the flame, due to the small radii of flame curvature at high perturbation frequencies.

This paper is organized as follows. Section II presents a simple set of experiments that were performed to reproduce the phenomenon and determine whether the trends were consistent with the hypothesis. Section III presents a theoretical analysis to describe the phenomenon. Section IV presents results that quantify the effects of flame geometry, disturbance field characteristics, perturbation frequency, and stretch sensitivity upon the flame's linear heat release response characteristics.

II. Experimental Observations

Although reported in the study by Bourehla and Baillot [17], no visual photographs of the filtering phenomenon appear to have been published. As such, images were obtained to illustrate this phenomenon and demonstrate that the qualitative trends were consistent with an unsteady stretch mechanism. These data were obtained with a 2.54-cm-diam, pilot-stabilized burner, previously described in Rajaram and Lieuwen [20]. Acoustic oscillations were excited with a loudspeaker placed at the bottom of the burner tube. The flame is stabilized with a methane-fueled (equivalence ratio of 1.15) annular pilot.

Experiments were performed with two fuels, propane and methane, which are thermodiffusively stable under lean and rich conditions, respectively. Consider first the lean propane result. Figure 1 illustrates two images of this flame when subjected to acoustic perturbations. In Fig. 1a, the flame front wrinkles symmetrically about the burner axis due to a convected wave traveling from the burner base to its tip, similar to a number of previous observations [6,7,17,21]. In Fig. 1b, the frequency is double that in Fig. 1a. The same flame wrinkles are clearly evident at the flame base, but they also have a shorter length scale and decay with axial location downstream. This, apparently, is the filtering phenomenon observed by Bourehla and Baillot [17]. Similarly, Fig. 2 plots the methane flame wherein the wrinkles decay for the rich case (thermodiffusively stable), whereas for the lean case the filtering phenomenon is not evident, consistent with our expectations.

From these results, we can conclude that this filtering phenomenon is associated with fuels and stoichiometries for which the flame exhibits a stretch sensitivity that acts to "smooth out" the wrinkles imposed by the acoustic forcing. This suggests that the previously hypothesized mechanism for the filtering phenomenon is due to the flame's stretch sensitivity. The rest of this paper describes the development of an analysis to quantitatively characterize this phenomenon.

III. Modeling Approach

The basic problem of interest is to determine the response of the flame position, $\tilde{\zeta}(\boldsymbol{x}, \tilde{t})$, and, in particular, the total heat release rate of the flame to a given disturbance velocity field, $\tilde{u}'(\boldsymbol{x}, \tilde{t})$. The global heat release rate of the flame is given by

$$Q(\tilde{t}) = \int_s \rho_1 S_L \Delta h_R \, \mathrm{d}A_{FL} \tag{1}$$

where the integral is performed over the flame surface, A_{FL}, and Δh_R is the heat release per unit mass of reactant. Also, several variables are presented in both dimensional and dimensionless form in this paper. To distinguish them, the superscript $\sim$ is used for the dimensional values of the variables r, t, u, v, and ζ. These same variables without a tilde are dimensionless, using the normalization scheme presented in the text following Eq. (7). Equation (1) shows the three fundamentally different ways of generating heat release disturbances in a premixed flame: fluctuations in mass burning rate ($\rho_1 S_L$), heat of reaction, or flame area. As noted by Clanet et al. [22], they can be

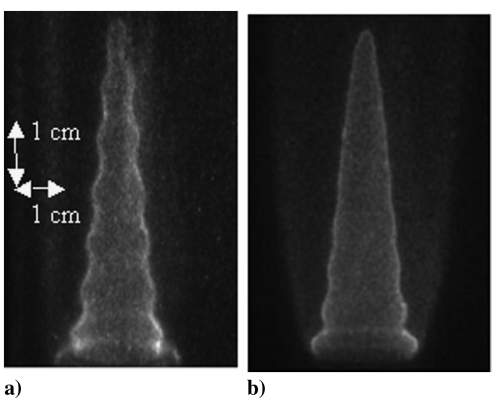

a) b)

Fig. 2 Visualization: a) 130 Hz acoustically excited lean methane flame (equivalence ratio = 0.8, $\tilde{\bar{u}} = 0.65$ m/s), and b) 140 Hz acoustically excited rich methane flame (equivalence ratio = 1.4, $\tilde{\bar{u}} = 0.7$ m/s, $\tilde{u}'/\tilde{\bar{u}} = 0.2$). Flow direction is upward.

classified based upon either their modification of the local internal structure of the flame (such as the local burning rate) or its global geometry (such as its area).

As we are focused upon the flame response to flow perturbations, we assume constant Δh_R and mixture density, ρ_1; analysis of the effects of these perturbations is given in Cho and Lieuwen [23] and McIntosh [24], respectively. Of course, if the flow perturbation is acoustic in origin, a density disturbance will accompany the velocity fluctuation. However, their relative impacts differ greatly, on the order of the flame speed Mach number. As such, our subsequent calculations focus upon the following quantity:

$$\frac{Q'}{\bar{Q}} = \frac{\int S'_L \, \mathrm{d}\bar{A}_{FL}}{\int \bar{S}_L \, \mathrm{d}\bar{A}_{FL}} + \frac{A'_{FL}}{\bar{A}_{FL}} \tag{2}$$

The flame curvature and hydrodynamic stretching introduced by the flow perturbations introduces perturbations in flame speed. In flames that are thermodiffusively stable (as assumed in this analysis), these unsteady stretch effects act to smooth out the flame front corrugation. This causes the amplitude of the flame wrinkle to diminish as it propagates along the flame. As the radius of flame wrinkling is approximately proportional to the inverse of the squared frequency, it can be anticipated that this effect grows in significance with frequency.

Figure 3 illustrates the geometry considered here, consisting of a two-dimensional wedge flame stabilized on a bluff body. The flame's axial and radial dimensions are given by the flame length, L_f, and radius, R. The instantaneous flame sheet location at the transverse location, $\tilde{r}$, is given by $\tilde{\zeta}(\tilde{r}, \tilde{t})$, assumed to be a single-valued function of $\tilde{r}$.

The analytical approach used here closely follows Ducruix et al. [25], Baillot et al. [26], and Fleifel et al. [8] The flame's dynamics are modeled with the front tracking equation [27]:

$$\frac{\partial \tilde{\zeta}}{\partial \tilde{t}} = \tilde{u} - \tilde{v}\frac{\partial \tilde{\zeta}}{\partial \tilde{r}} - S_L\sqrt{\left(\frac{\partial \tilde{\zeta}}{\partial \tilde{r}}\right)^2 + 1} \tag{3}$$

where $\tilde{u}$ and $\tilde{v}$ denote the axial and radial velocity components, and S_L is the laminar flame speed.

The flame speed can be expressed as [13,14,27]

$$S_L = S_{L,o}\,(1 - M_{a,c}\,C + M_{a,s}H) \tag{4}$$

The expressions for curvature (C) and hydrodynamic strain (H) are given by

$$C = -\nabla \cdot \boldsymbol{n} \qquad H = \frac{\boldsymbol{n} \cdot \nabla \times (\tilde{\boldsymbol{V}}|_{\tilde{y}=\tilde{\zeta}} \times \boldsymbol{n}) - (\tilde{\boldsymbol{V}}_f \cdot \boldsymbol{n})(\nabla \cdot \boldsymbol{n})}{S_{L,o}} \tag{5}$$

where $\boldsymbol{n}$ is the unit vector normal to the flame front pointing toward the unburnt gases, $\tilde{\boldsymbol{V}}_f$ denotes the local velocity of the flame front, and $S_{L,o}$ is the flame speed in the absence of stretch effects. In the general unsteady case, $M_{a,c}$ and $M_{a,s}$ must be interpreted as

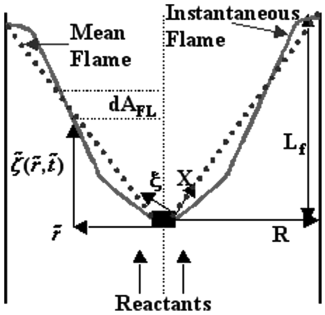

Fig. 3 Illustration of two-dimensional wedge-shaped flame geometry stabilized on a bluff body. The dotted and solid lines illustrate the mean and instantaneous flame locations, respectively. Flow direction is upward.

Markstein linear integral operators with timewise kernels [13,14] [or frequency-dependent transfer functions when put in the frequency domain; see Eq. (6)] for curvature and hydrodynamic strain, respectively. Defining $(S_L/S_{L,o} - 1)$ as m, and then taking the Fourier transform (denoted by $\hat{}$ quantities) of the flame speed relation gives [13,14]

$$\hat{m} = -\hat{M}_{a,c}\hat{C} + \hat{M}_{a,s}\,\hat{H} \tag{6}$$

In the quasi-steady case, these transfer functions (both $\hat{M}_{a,c}$ and $\hat{M}_{a,s}$) reduce to the Markstein length, M_a. For single-step kinetics, Joulin [13] has shown that these Markstein transfer functions can be characterized by a Strouhal number and a scaled Lewis number, le, defined as

$$le = Ze\,[1 - (1/Le)] \tag{7}$$

where Le and Ze refer to the Lewis and Zeldovich numbers, respectively.

The variables $\tilde{t}$, $\tilde{r}$, $\tilde{u}$, and $\tilde{\zeta}$ are nondimensionalized by $\bar{\tilde{u}}/L_f$, R, $\bar{\tilde{u}}$, and L_f (note that the value of L_f and R refer to their nominal values without imposed oscillations), where $\bar{\tilde{u}}$ is the mean axial velocity. They are related to the nominal flame speed and average flow velocity by

$$\bar{\tilde{u}}/S_{L,o} = \sqrt{(L_f/R)^2 + 1} \tag{8}$$

The ratio of the flame length to radius plays an important role in the flame's dynamics and is denoted by β:

$$\beta = L_f/R \tag{9}$$

Following previous studies [8,26], we assume that the flame remains anchored at the base, that is,

$$\tilde{\zeta}(\tilde{r} = 0, \tilde{t}) = 0 \tag{10}$$

For wedge flames, the second boundary condition comes from the characteristic boundary condition that all information should propagate out of the flame; information should not propagate into the flame from this end. This is a rigorous way of capturing the fact that the flame tip is free to move around (see Fig. 3), that is,

$$\frac{\partial^2 \tilde{\zeta}(\tilde{r} = R, \tilde{t})}{\partial \tilde{r}^2} = 0 \tag{11}$$

The governing equation for the dynamics of 2-D conical flames is identical to that of wedge flames except for the boundary condition in Eq. (11); that is, Eq. (11) is replaced by the condition that the flame is symmetric about the axis. For axisymmetric flames (conical and wedge), there is an additional stretch term due to the azimuthal component, which introduces additional analytical difficulties. This point and the results for such cases are presented in [28].

Experimental studies have clearly shown that the disturbance field can exhibit a variety of characteristics, including both acoustic and vortical components, which in the latter case exhibit phase variations over a convective wavelength, $\bar{\tilde{u}}/f$ [28,29]. As such, we assume the disturbance field to have an arbitrary phase velocity, so that the velocity field is specified as follows:

$$\tilde{u}(\tilde{\zeta}, \tilde{t}) = Re(\bar{\tilde{u}} + \tilde{u}'\, e^{i(k\tilde{\zeta} - \omega_o \tilde{t})}) \tag{12}$$

Here the convective wave number k is defined as follows:

$$k = (\omega_o/\tilde{u}_c) = (\bar{\tilde{u}}/\tilde{u}_c)(\omega_o/\bar{\tilde{u}}) = K(\omega_o/\bar{\tilde{u}}) \tag{13}$$

where $\tilde{u}_c$ is defined as the phase velocity of the disturbance, and ω_o denotes the angular frequency of the velocity disturbance. K is a parameter that denotes the ratio of the mean flow velocity to the phase velocity of the disturbances.

The nondimensionalized velocity field is then given by

$$u(\zeta, t) = Re(1 + \varepsilon\, e^{i(St(K\zeta - t))}) \tag{14}$$

where the Strouhal number is

$$St = \omega_o L_f / \tilde{\bar{u}} \tag{15}$$

and the velocity perturbation is

$$\varepsilon = \tilde{u}'/\tilde{\bar{u}} \tag{16}$$

The velocity is assumed to be purely axial, which implies that the velocity field is not incompressible (for $K \neq 0$). Extending the current model to include a radial velocity component so as to be incompressible is straightforward. However, it makes the algebra quite tedious and does not provide essential new insights into the linearized flame physics. It is emphasized that our goal here is not to simulate the exact disturbance field of any particular experimental setup, but rather to elucidate the key physical processes and nondimensional parameters that influence the flame's dynamics.

IV. Results and Discussion

In this section, we derive an expression for the flame heat release–velocity transfer function that incorporates the effect of disturbances with arbitrary phase velocity and stretch-dependent flame speed.

The flame position is expanded as [26]

$$\zeta(r, t) = \zeta_o(r) + \zeta'(r, t) \qquad \zeta'(r, t) = \zeta_1(r, t)\varepsilon + \mathcal{O}(\varepsilon^2) \tag{17}$$

The mean flame shape in the absence of perturbations is given by

$$\zeta_o(r) = r \tag{18}$$

Using Eqs. (3), (6), (17), and (18), the evolution equation for ζ_1 is

$$\frac{\hat{\sigma}_c \beta}{(1+\beta^2)^{3/2}} \frac{\partial^2 \zeta_1}{\partial r^2} - \frac{\beta^2}{1+\beta^2} \frac{\partial \zeta_1}{\partial r} + iSt\, \zeta_1 + \left(1 - \frac{i\hat{\sigma}_s K St \beta}{\sqrt{1+\beta^2}}\right) e^{iSt\ \{Kr\}} = 0 \tag{19}$$

where

$$(\hat{\sigma}_c, \hat{\sigma}_s) = \left(\frac{\hat{M}_{a,c}}{R}, \frac{\hat{M}_{a,s}}{R}\right) \tag{20}$$

The solution of Eq. (19) given the boundary conditions in Eq. (10) and (11) is

$$\zeta_1 = Re\left(\frac{(i + \eta St_2\, \sigma_s^*) e^{-iSt\ t}}{St(i\alpha - i\alpha\eta - \sigma_c^* \eta^2 St)} \times \left(i\alpha e^{\frac{i\eta St\ r}{\alpha}} + \frac{(2\eta^2 St^2 \sigma_c^{*2}(e^{-\frac{\Lambda}{\sigma_c^*} + \frac{(-1+\Lambda)(1-r)}{2\sigma_c^*} + \frac{i\eta St}{\alpha}} - e^{-\frac{(1+\Lambda)(1-r)}{2\sigma_c^*} + \frac{i\eta St}{\alpha}}) + \alpha(-\alpha + \alpha\Lambda + 2i\sigma_c^* St) e^{\frac{(1-\Lambda)}{2\sigma_c^*} - \frac{(1+\Lambda)(1-r)}{2\sigma_c^*}} + \alpha(\alpha + \alpha\Lambda - 2i\sigma_c^* St) e^{\frac{r(1-\Lambda)}{2\sigma_c^*}})}{(i(-\alpha + \alpha\Lambda + 2i\sigma_c^* St) e^{\frac{-\Lambda}{\sigma_c^*}} + (i\alpha + i\alpha\Lambda + 2\sigma_c^* St))}\right)\right) \tag{21}$$

where

$$\eta = K\alpha \tag{22}$$

$$\alpha = \beta^2/(\beta^2 + 1) \tag{23}$$

$$\sigma_c^* = \frac{\hat{\sigma}_c}{\beta\sqrt{1+\beta^2}} \tag{24}$$

$$\sigma_s^* = \frac{\hat{\sigma}_s \beta}{\sqrt{1+\beta^2}} \tag{25}$$

$$\Lambda = \sqrt{1 - 4i\hat{\sigma}_c St/\alpha} \tag{26}$$

The flame front position [see Eq. (21)] can be interpreted as the superposition of the flame disturbances created at each point due to flow nonuniformity and disturbances originating from the flame base that are convected along the flame front [7]. In most cases of practical interest, the Markstein length is much smaller than the characteristic geometric length scale, that is, $\hat{\sigma}_c, \hat{\sigma}_s \ll 1$. In this limit, Eq. (21) can be written as

$$\zeta_1 = Re\left((i + \eta St_2\, \sigma_s^*) e^{-iSt\ t} (e^{iSt_2 r} e^{-\sigma_c^* St_2^2 r} - e^{i\eta St_2 r}) \times \left(\frac{1}{(\eta - 1)St} + \frac{i\sigma_c^* \eta^2}{\alpha(\eta - 1)^2}\right)\right) + \mathcal{O}(\sigma^{*2}) \tag{27}$$

For a spatially uniform disturbance ($\eta \to 0$), Eq. (27) simplifies to

$$\lim_{\eta \to 0} \zeta_1 = Re\left(e^{-iSt\ t} \frac{i}{St}(1 - e^{iSt_2 r} e^{-\sigma_c^* St_2^2 r})\right) + \mathcal{O}(\sigma^{*2}) \tag{28}$$

Next, consider the total heat release of the flame, obtained using Eq. (2). The first term is entirely due to fluctuations of the flame speed and can be expressed as

$$\frac{\int S_L' \,\mathrm{d}\bar{A}}{\int \bar{S}_L \,\mathrm{d}\bar{A}} = \varepsilon\sigma_s^*(u'(r=0,t) - u'(r=1,t)) + \varepsilon\sigma_c^* \alpha\left(\frac{\partial \zeta_1(r=0,t)}{\partial r} - \frac{\partial \zeta_1(r=1,t)}{\partial r}\right) \tag{29}$$

To evaluate the second term in Eq. (2), note that the nondimensionalized surface area for a two-dimensional wedge flame is given by

$$\frac{A(t)}{\bar{A}} = \frac{\int_0^1 \sqrt{1 + \beta^2 (\frac{\partial \zeta}{\partial r})^2}\,\mathrm{d}r}{\sqrt{1+\beta^2}} \tag{30}$$

Substituting Eqs. (17), (18), (21), and (30) in Eq. (2) and defining $G = \frac{Q'/\bar{Q}}{\bar{u}'/\bar{u}}$ yields

$$G(St_2, \eta, \sigma_c^*, \sigma_s^*) = \overbrace{G_{S_L}}^{S_L\ \text{Fluctuation}} + \overbrace{G_{\text{Area}}}^{\text{Area Fluctuation}} \tag{31}$$

where the contribution due to S fluctuations is

$$G_{S_L} = (e^{i\,\eta St_2} - 1)\sigma_s^* + \frac{(i+\sigma_s^*)(I_1+I_2)}{2St_2\,(-i+i\eta+\sigma_c^*\eta^2 St_2)(i(-1+\Lambda+2i\sigma_c^* St_2)e^{\frac{-\Lambda}{\sigma_c^*}} + (i+i\Lambda+2\sigma_c^* St_2))} \tag{32}$$

where

$$I_1 = (1+\Lambda-2i\sigma_c^* St_2)(-1+\Lambda+2i\eta\sigma_c^* St_2) + 4\Lambda\eta^2\sigma_c^{*2}St_2^2 e^{i\,\eta St_2 - \frac{1+\Lambda}{2\sigma_c^*}} - 2\eta\sigma_c^* St_2(i+(\Lambda+2)\sigma_c^* St_2 + \Lambda(i+\eta\sigma_c^* St_2))e^{i\,\eta St_2}$$

$$I_2 = 4i\Lambda\sigma_c^* St_2 e^{\frac{1-\Lambda}{2\sigma_c^*}} - 2e^{i\,\eta St_2 - \frac{\Lambda}{\sigma_c^*}}\eta\sigma_c^* St_2(-i-(\Lambda+2)\sigma_c^* St_2 + \Lambda(i+\eta\sigma_c^* St_2)) + (1+\Lambda-2i\eta\sigma_c^* St_2) \times (-1+\Lambda+2i\sigma_c^* St_2)e^{-\frac{\Lambda}{\sigma_c^*}}$$

G_{Area} can be written in the following form:

$$G_{\text{Area}} = (i+\eta St_2\sigma_s^*)\frac{(e^{i\eta St_2}(1+\Lambda-2i\sigma_c^* St_2+2\sigma_c^{*2}\eta^2 St_2^2) - 2\Lambda e^{\frac{1-\Lambda}{2\sigma_c^*}} + e^{i\eta St_2 - \frac{\Lambda}{\sigma_c^*}}(-1+\Lambda+2i\sigma_c^* St_2 - 2\sigma_c^{*2}\eta^2 St_2^2))}{St_2(-i+i\eta+\sigma_c^*\eta^2 St_2)(i(-1+\Lambda+2i\sigma_c^* St_2)e^{\frac{-\Lambda}{\sigma_c^*}} + (i+i\Lambda+2\sigma_c^* St_2))} \tag{33}$$

where

$$St_2 = \frac{St}{\alpha} = \frac{St(1+\beta^2)}{\beta^2} \tag{34}$$

These two expressions reduce to the following in the small Markstein length limit:

$$G_{\text{Area}} = i\frac{e^{iSt_2} - e^{i\eta St_2}}{(\eta-1)St_2} + \underbrace{\frac{\eta(e^{iSt_2} - e^{i\eta St_2})}{(\eta-1)}\sigma_s^*}_{\text{Hydrodynamic Strain}} + \underbrace{\frac{(\eta^2 e^{i\eta St_2} - e^{iSt_2}((\eta-1)iSt_2+\eta^2))}{(\eta-1)^2}\sigma_c^*}_{\text{Curvature}} + \mathcal{O}(\sigma^{*2})$$

$$G_{SL} = \underbrace{(e^{i\,\eta St_2}-1)\sigma_s^*}_{\text{Hydrodynamic Strain}} + \underbrace{\frac{(\eta-1+e^{iSt_2}-\eta e^{i\eta St_2})}{(\eta-1)}\sigma_c^*}_{\text{Curvature}} + \mathcal{O}(\sigma^{*2}) \tag{35}$$

Furthermore, for a spatially uniform disturbance ($\eta \to 0$), Eq. (35) reduces to

$$\lim_{\eta\to 0} G_{\text{Area}} = i\frac{1-e^{iSt_2}}{St_2} + \underbrace{iSt_2 e^{iSt_2}\sigma_c^*}_{\text{Curvature}} + \mathcal{O}(\sigma^{*2})$$
$$\lim_{\eta\to 0} G_{SL} = \underbrace{(1-e^{iSt_2})\sigma_c^*}_{\text{Curvature}} + \mathcal{O}(\sigma^{*2}) \tag{36}$$

These results reduce to previously developed transfer functions [5] when $\sigma_{c,s}^* = 0$ and $K = 0$ (i.e., for a uniform disturbance field model without flame stretch). Thus, the linear flame transfer function, Eq. (31), depends upon four key parameters: St_2, η, σ_c^*, and σ_s^*. St_2 combines the effect of flame aspect ratio and Strouhal number; see Eq. (34). It is useful to define a Strouhal number based upon the convective velocity ($\tilde{u}_c$) of the flow disturbances, St_c, which naturally arises in the two transfer functions [Eq. (31)] and equals ηSt_2:

$$\eta St_2 = KSt = \left(\frac{\tilde{\bar{u}}}{\tilde{u}_c}\right)\left(\frac{\omega_o L_F}{\tilde{\bar{u}}}\right) = \frac{\omega_o L_F}{\tilde{u}_c} = St_c \tag{37}$$

These two Strouhal numbers are related to the amount of time taken for a flow (St_c) and flame front (St_2) disturbance (which is ultimately created by a flow disturbance) to propagate the flame length, normalized by the acoustic period.

Curvature and hydrodynamic strain effects are incorporated through the dimensionless frequency-dependent Markstein transfer functions, σ_c^* and σ_s^*, respectively. For the constant density case, Joulin [13] has derived the following expressions:

$$\hat{\sigma}_c = \frac{\delta}{R}\frac{(1+\frac{le}{2}\frac{\Omega_+}{\chi})}{(1+\frac{le}{2}\frac{\Omega_-}{\chi})}; \qquad \hat{\sigma}_s = \frac{\delta}{R\Omega_+}\frac{(1+\frac{le}{2}\frac{1}{\chi})}{(1+\frac{le}{2}\frac{\Omega_-}{\chi})};$$
$$\Omega_\pm = \frac{1\pm\sqrt{\chi}}{2}; \qquad \chi = 1+4iSt\frac{\delta}{R}\frac{\sqrt{1+\beta^2}}{\beta} \tag{38}$$

where δ is the flame thickness. In particular, note that, for the quasi-steady state case, both the transfer functions reduce to the nondimensionalized Markstein length σ, that is,

$$\hat{\sigma}_c(St=0, le) = \hat{\sigma}_s(St=0, le) = Ma/R = \sigma \tag{39}$$

Also, for the quasi-steady case, we will denote σ^* as

$$\sigma^* = \frac{\sigma}{\beta\sqrt{1+\beta^2}} \tag{40}$$

A. Baseline Flame Response

Flame speed fluctuations are neglected in this section to illustrate baseline flame response characteristics. For this case, the transfer function expression simplifies to

$$\lim_{\sigma^*\to 0} G = i\frac{e^{iSt_2} - e^{i\eta St_2}}{(\eta-1)St_2} \tag{41}$$

The dependence of the magnitude and phase of the wedge flame transfer function $G(St_2, \eta, \sigma^* = 0)$ upon St_2 at several η values is plotted in Figs. 4 and 5, respectively. Consider the magnitude results first. Note that all gain values tend toward unity at low St_2. Moreover, the gain value is always less than one (except for the $\eta = 1$ case) and exhibits a series of peaks and nodes as shown in Fig. 4. The gain (not

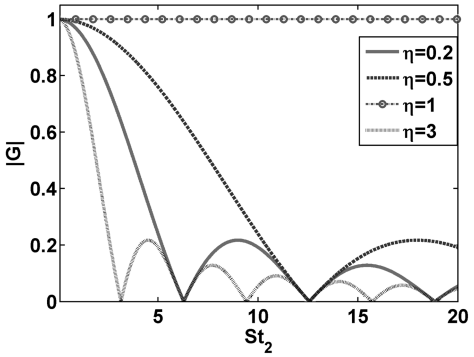

Fig. 4 Strouhal number dependence of the magnitude of the wedge transfer function for different values of η, $\sigma^* = 0$.

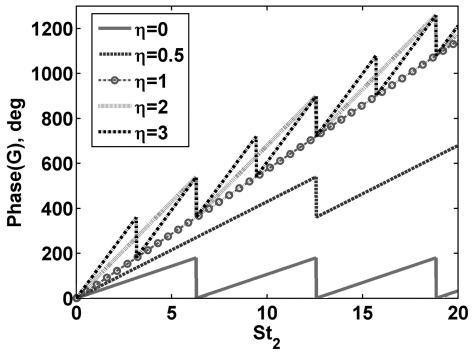

Fig. 5 Strouhal number dependence of the phase of the transfer function for different values of η, $\sigma^* = 0$.

phase) for the $\eta = 0$ and 2 cases are identical, which can be anticipated from the η dependence of the gain in Eq. (41). In particular, the nodes in the gain satisfy the condition that $|\eta\ St_2 - St_2| = 2n\pi$. Although the locations of the nodes and peaks are dependent on η and St_2, the magnitude of the peaks is only a function of St_2 and independent of η [can be deduced from Eq. (41)].

As discussed in the Introduction, for a spatially uniform disturbance ($\eta \to 0$), the flame dynamics is controlled exclusively by the boundary condition term, whereas for a spatially nonuniform disturbance ($\eta \neq 0$) the response is determined by the constructive (peaks) or destructive (nodes) superpositions of the homogeneous and particular solutions. This explains the η dependence of the nodes and the peaks. However, in contrast to the axisymmetric flames (conical and wedge) [7], a two-dimensional wedge flame exhibits nodes/peaks even for $\eta \to 0$, as indicated in Fig. 4.

The limit of $\eta \to 1$ corresponds to the exact coincidence of flame front and flow disturbance velocity, leading to a case wherein the two dimensionless Strouhal numbers, ηSt_2 and St_2, reduce to a single one, represented by the term St_2. For this case, the transfer function simplifies to

$$\lim_{\sigma^* \to 0, \eta \to 1} G = e^{iSt_2} \tag{42}$$

This leads to the result wherein the gain is constant and equal to unity irrespective of the Strouhal number. In reality, unsteady stretch effects play a major role in this case, as discussed in the next section. The transfer function phase (see Fig. 5) starts at 0 deg at low St_2 and increases monotonically with St_2. For all other η values, although the phase increases with St_2, there is a 180 deg phase shift at frequencies corresponding to the nodal locations in the gain.

B. Unsteady Stretch Effects

The influence of stretch on the flame transfer function gain and phase is considered in this section. To obtain insight into the results, it is useful to first consider the uniform disturbance velocity field ($\eta = 0$) case. Note that for this case, flame speed modification occurs only due to curvature [not hydrodynamic strain; see Eq. (19)].

To illustrate the effect of flame speed modification on the flame shape, the deviation of the flame front from its average position is shown in Fig. 6. The point $X = 0$ in Fig. 6 corresponds to the point of attachment at the flame base (see Fig. 3). In the constant flame speed case ($\sigma^* = 0$), the flame front exhibits sinusoidal wrinkling [21]. However, in the presence of stretch, the amplitude of the flame front perturbation decays continuously from the flame base to the tip; see Fig. 6. This feature, wherein the oscillations on the flame front are only evident at the flame base and become strongly damped at axial locations downstream, is clearly evident in Fig. 1 and also consistent with the experimental observations of Bourehla and Baillot [17]. They observed this phenomenon for an axisymmetric conical flame under conditions corresponding to $St > 38$, $\beta = 2$, and $\sigma^* \sim 0.005$, the same conditions simulated in Fig. 6. The strong damping in the flame front oscillations away from the flame base (at the same conditions), an effect that grows with σ^*, is clearly captured in Fig. 6. Furthermore, as shown in Eq. (28), this damping of the flame wrinkling amplitude scales [16] as $e^{-\sigma_c^* St_2^2 r}$. Note that the dissipation in flame wrinkling scales as the square of the frequency.

As discussed in the context of Eq. (2), the total heat release rate is determined by the fluctuations in the flame surface area and flame speed. Considering only leading-order stretch terms in Eq. (31), the flame transfer function expression for the uniform velocity case ($\eta = 0$) can be simplified to Eq. (36). The individual contributions to the transfer function are denoted by G_{Area} and G_{SL}, respectively. It can be inferred from Eq. (36) that curvature effects become important for G_{Area} when $|\sigma_c^*|St_2 \sim \mathcal{O}(1/St_2)$, that is, $|\sigma_c^*|St_2^2 \sim \mathcal{O}(1)$. However, as noted by Wang et al. [30], flame speed fluctuations become the dominant contributor to heat release fluctuations at higher frequencies, that is, when $|\sigma_c^*|St_2 \sim \mathcal{O}(1)$. These trends can be clearly observed in the gain and phase of the heat release transfer function illustrated in Figs. 7 and 8, respectively. Comparing the stretched ($G_{\sigma^*=0.05}$) and unstretched ($G_{\sigma^*=0}$) cases, it can be inferred that for lower Strouhal numbers (i.e., $|\sigma_c^*|St_2^2 \sim \mathcal{O}(1)$) the total transfer function ($G_{\sigma^*=0.05}$) is very close to $G_{\text{Area},\sigma^*=0.05}$, implying that the contribution from the curvature-affected flame area fluctuations dominates over that of the flame speed fluctuations. The contribution from flame speed fluctuations ($G_{SL,\sigma^*=0.05}$) starts from zero and grows in significance with Strouhal number. At lower Strouhal numbers it is out of phase with $G_{\text{Area},\sigma^*=0.05}$ (see Fig. 8), causing the overall gain ($G_{\sigma^*=0.05}$) to be lower (see Fig. 7) than in the unstretched case ($G_{\sigma^*=0}$). As the Strouhal number increases, the length scale of wrinkling decreases, leading to a growth in the significance of curvature effects. As such, the flame front wrinkles progressively damp as they propagate away from the flame base (see Fig. 6), leading to a reduction in the gain due to the flame area fluctuations. With a further increase in Strouhal number (i.e., $|\sigma_c^*|St_2 \sim \mathcal{O}(1)$), the relative importance of the flame speed fluctuations grows with Strouhal number and becomes comparable to the flame area fluctuations.

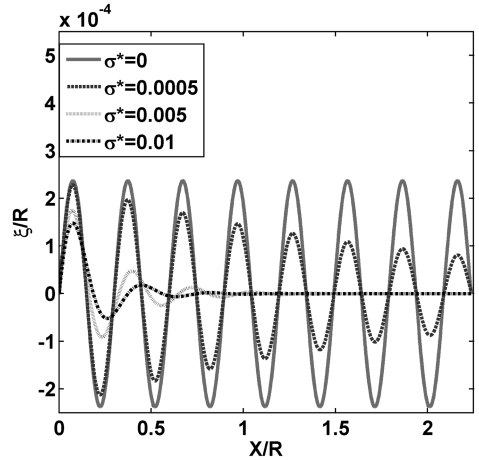

Fig. 6 Instantaneous wedge flame shape with X axis along the mean flame front. $\beta = 2$, $St = 38$, $\eta = 0$, $le = 0$.

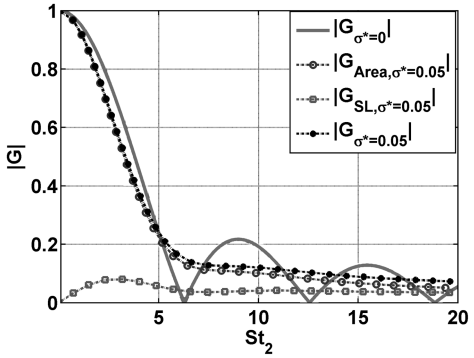

Fig. 7 Effect of stretch on the Strouhal number dependence of the magnitude of the transfer functions due to area (G_{Area}) and S_L fluctuations (G_{SL}), $\eta = 0$, $le = 0$.

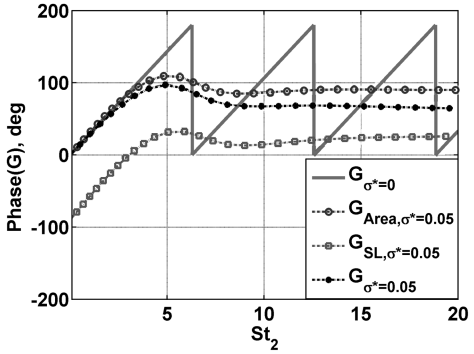

Fig. 8 Effect of stretch on the Strouhal number dependence of the phase of the transfer functions due to area (G_{Area}) and S_L fluctuations (G_{SL}), $\eta = 0$, $le = 0$.

Another striking feature is the absence of nodes in the gain (see Fig. 7). For $St_2 \sim 2n\pi$, corresponding to nodes in $G_{\sigma^*=0}$, curvature effects cause $G_{\sigma^*=0.05}$ to be higher than in the unstretched case. This is also evident in Fig. 8, wherein the 180 deg jumps in the phase of $G_{\sigma^*=0}$ are smoothened out. This is due to the fact that the nodal response of the flame tip disappears at $St_2 = 2n\pi$ (present in the unstretched case), leading to an increase in the bulk flame area oscillation. Hence, curvature effects cause a reduction in the gain in comparison to the unstretched case, except for nodes, in the response of the unstretched case. These trends grow with increasing values of σ^*.

In the more general case of a nonuniform disturbance velocity field ($\eta \neq 0$), the flame speed modification occurs through both curvature and hydrodynamic strain effects. However, the Strouhal number dependence of the two Markstein transfer functions is different. At high Strouhal numbers, σ_c^* reaches a constant limiting value whereas σ_s^* decays as $\sim 1/\sqrt{St}$ [see Eq. (38)]. Considering only leading-order stretch terms in Eq. (31), the flame transfer function expression can be simplified to Eq. (35). As noted earlier in the context of Eq. (36), the primary contribution to the transfer function at low Strouhal numbers comes from G_{Area}. Moreover, it can be inferred from Eq. (35) that curvature effects become important for G_{Area} when $|\sigma_c^*|St_2^2 \sim \mathcal{O}(1)$, whereas strain effects become prominent only when $|\sigma_s^*| \sim \mathcal{O}(1/St_2)$. Hence, at low Strouhal numbers, unsteady curvature effects dominate over those of hydrodynamic strain for G_{Area}. At high Strouhal numbers (i.e. $|\sigma_c^*, \sigma_s^*|St_2 \sim \mathcal{O}(1)$), the contribution from G_{SL} becomes comparable to G_{Area}. Also, the *relative* contribution from hydrodynamic strain and curvature are of the same order for both G_{Area} and G_{SL}. However, because σ_s^* decays with an increase in Strouhal number [see Eq. (38)], the curvature effects may still have a higher total contribution to G_{SL}.

Figure 9 shows the magnitude of the flame transfer function for a case with phase speed corresponding to $\eta = 2$. Clearly, the contribution from G_{SL} becomes significant with increasing Strouhal

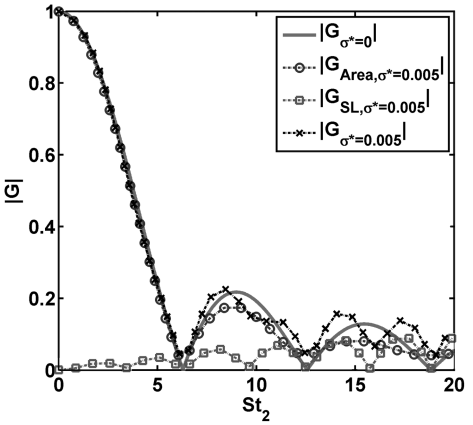

Fig. 9 Effect of stretch on the Strouhal number dependence of the magnitude of the transfer functions due to area (G_{Area}) and S_L fluctuations (G_{SL}), $\eta = 2$, $le = 0$.

numbers and, in fact, is greater than the contribution from G_{Area} at certain Strouhal numbers. However, the phase of the flame transfer function (see Fig. 10) for $G_{\sigma^*=0.005}$ follows that of $G_{\text{Area},\sigma^*=0.005}$. In summary, at high Strouhal numbers, G_{SL} can be as significant as G_{Area} and can cause the flame transfer function magnitude to be greater than in the unstretched case.

An important feature of the flame dynamics is the response at $\eta = 1$. In contrast to the constant gain of unity exhibited in the unstretched case (see Fig. 4), stretch effects cause the gain to reduce monotonically with increasing Strouhal number. Also, note that, in the unstretched case, the gain for the $\eta = 0$ and 2 cases is identical as it is inversely proportional to $|\eta - 1|$ [see Eq. (41)]. However, at higher Strouhal numbers, stretch effects cause the gains for the two cases to differ considerably.

This theoretical analysis has been applied to 2-D wedge flames. In closing, we discuss the manner in which these results vary with other geometries. As noted earlier, 2-D conical flames have a different boundary condition at the flame tip. This introduces an exponentially small correction to the mean flame shape near the tip, $\exp(-1/\sigma_c^*)$. In the limit of small σ, this term is smaller than all powers of σ (i.e., $\lim_{\sigma^* \to 0} e^{-\frac{1}{\sigma^*}} < \sigma^{*n}$, where n is any integer) and can be neglected. Thus, the discussion in the previous section is equally valid for 2-D conical flames, assuming thin flames relative to the burner diameter.

We next consider axisymmetric geometries. The flame response equation includes an additional azimuthal stretch term, proportional to $\frac{1}{r}\frac{\partial \xi_1}{\partial r}$. In the physically interesting case of $\sigma \ll 1$, the stretch term is only significant at high frequencies wherein the length scale of wrinkling is small, that is, conditions under which the second derivative of flame curvature [included in our analysis; see Eq. (19)] has a much larger value than the first derivative. As such, this

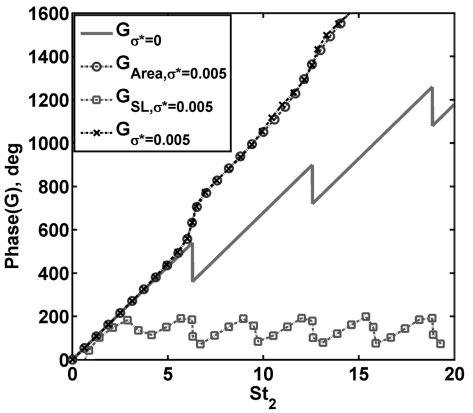

Fig. 10 Effect of stretch on the Strouhal number dependence of the phase of the transfer functions due to area (G_{Area}) and S_L fluctuations (G_{SL}), $\eta = 2$.

azimuthal curvature term is only nonnegligible near $r = 0$. However, the portion of flame area near $r = 0$ is negligible relative to that contributed by the rest of the flame. As such, the trends described in this paper apply in most situations to the *flame position* for axisymmetric flames as well (see [31] for results). However, although the response of the flame position is quite similar to the results discussed earlier in this section, the effect of flame geometry causes the response of the *overall heat release* to exhibit significant quantitative differences from the 2-D geometry. These differences are due to the fact that unsteady curvature effects grow in prominence with downstream distance. Thus, for an axisymmetric wedge flame for which the majority of the flame area is at its tip, curvature effects cause substantial reductions in flame response relative to those for the 2-D case (in which flame area is distributed equally along the whole flame length). In contrast, for a conical flame, the majority of the flame area lies at the flame base, where curvature effects are not as significant. Thus, curvature effects influence the area fluctuations (G_{Area}) of these flames only at much higher frequencies than for axisymmetric wedge flames. In contrast, strain effects are equally important for all the flame configurations and will contribute to the total heat release response through the flame speed fluctuations (G_{SL}).

V. Conclusions

This study shows that experimentally observed decay in flame wrinkles with downstream distance can be captured by analyses including unsteady curvature effects. The variation in flame speed along the flame front acts to smoothen out the short length scale wrinkles. This effect becomes significant when $|\sigma_c^*|St_2^2 = \frac{4\pi^2|\hat{M}_c|\ f^2 L_f}{\bar{u}^2\sqrt{\beta^2+1}} \sim \mathcal{O}(1)$, which implies that the Markstein transfer function for curvature, flame aspect ratio, flame length, and mean flow velocity are the critical parameters determining the frequency at which unsteady curvature effects become important. Curvature effects impact the heat release response primarily through flame area oscillations. At higher Strouhal numbers ($|\sigma_c^*\sigma_s^*|St_2 \sim \mathcal{O}(1)$), both hydrodynamic strain and curvature effects cause flame speed fluctuations to become as significant as the flame area fluctuations, which can cause the total heat release gain to be *greater* than in the unstretched case in certain instances.

References

[1] Lieuwen, T., "Physics of Premixed Combustion-Acoustic Wave Interactions," *Combustion Instabilities in Gas Turbine Engines*, edited by T Lieuwen, and V. Yang, AIAA, Reston, VA, 2005, Chap. 12.

[2] Paschereit, C. O., Gutmark, E., and Weisenstein, W., "Control of Thermoacoustic Instabilities and Emissions in an Industrial-Type Gas-Turbine Combustor," *Proceedings of the Combustion Institute*, Vol. 27, 1998, pp. 1817–1824. doi:10.1016/S0082-0784(98)80023-4

[3] Dowling, A. P., and Stow, S. R., "Acoustic Analysis of Gas Turbine Combustors," *Journal of Propulsion and Power*, Vol. 19, No. 5, 2003, pp. 751–764. doi:10.2514/2.6192

[4] Broda, J. C., Seo, S., Santoro, R. J., Shirhattikar, G., and Yang, V., "An Experimental Study of Combustion Dynamics of a Premixed Swirl Injector," *Proceedings of the Combustion Institute*, Vol. 27, 1998, pp. 1849–1856. doi:10.1016/S0082-0784(98)80027-1

[5] Lieuwen, T., "Nonlinear Kinematic Response of Premixed Flames to Harmonic Velocity Disturbances," *Proceedings of the Combustion Institute*, Vol. 30, No. 2, 2005, pp. 1725–1732. doi:10.1016/j.proci.2004.07.020

[6] Schuller, T., Durox, D., and Candel, S., "A Unified Model for the Prediction of Laminar Flame Transfer Functions—Comparisons Between Conical and V-Flame Dynamics," *Combustion and Flame*, Vol. 134, Nos. 1–2, 2003, pp. 21–34. doi:10.1016/S0010-2180(03)00042-7

[7] Preetham, Santosh, H., and Lieuwen, T., "Dynamics of Laminar Premixed Flames Forced by Harmonic Velocity Disturbances," *Journal of Propulsion and Power*, Vol. 24, No. 6, 2008, pp. 1390–1402. doi:10.2514/1.35432

[8] Fleifel, M., Annaswamy, A. M., Ghoniem, Z. A., and Ghoniem, A. F., "Response of a Laminar Premixed Flame to Flow Oscillations: A Kinematic Model and Thermoacoustic Instability Results," *Combustion and Flame*, Vol. 106, No. 4, 1996, pp. 487–510. doi:10.1016/0010-2180(96)00049-1

[9] Saitoh, T., and Otsuka, Y., "Unsteady Behavior of Diffusion Flames and Premixed Flames for Counterflow Geometry," *Combustion Science and Technology*, Vol. 12, 1976, pp. 135–146. doi:10.1080/00102207608946713

[10] Im, H. G., Bechtold, J. K., and Law, C. K., "Response of Counterflow Premixed Flames to Oscillating Strain Rates," *Combustion and Flame*, Vol. 105, 1996, pp. 358–372. doi:10.1016/0010-2180(95)00217-0

[11] Huang, Z., Bechtold, J. K., and Matalon, M., "Weakly Stretched Premixed Flames in Oscillating Flows," *Combustion Theory and Modelling*, Vol. 2, No. 2, 1998, pp. 115–133. doi:10.1088/1364-7830/2/2/001

[12] Egolfopoulos, F. N., "Dynamics and Structure of Unsteady, Strained, Laminar Premixed Flames,"*Proceedings of the Combustion Institute*, Vol. 25, 1994, pp. 1365–1373. doi:10.1016/S0082-0784(06)80779-4

[13] Joulin, G., "On the Response of Premixed Flames to Time Dependent Stretch and Curvature," *Combustion Science and Technology*, Vol. 97, 1994, pp. 219–229. doi:10.1080/00102209408935375

[14] Clavin, P., and Joulin, G., "High Frequency Response of Premixed Flames to Weak Stretch and Curvature: A Variable Density Analysis," *Combustion Theory and Modelling*, Vol. 1, No. 4, 1997, pp. 429–446. doi:10.1080/713665342

[15] Im, H. G., and Chen, J. H., "Effects of Flow Transients on the Burning Velocity of Laminar Hydrogen/Air Premixed Flames," *Proceedings of the Combustion Institute*, Vol. 28, 2000, pp. 1833–1840. doi:10.1016/S0082-0784(00)80586-X

[16] Wang, H., "Oscillation and Extinction in Flames," Ph.D. Thesis, Princeton Univ., Princeton, NJ, 2007.

[17] Bourehla, A., and Baillot, F., "Appearance and Stability of a Laminar Conical Premixed Flame Subjected to an Acoustic Perturbation," *Combustion and Flame*, Vol. 114, Nos. 3–4, 1998, pp. 303–318. doi:10.1016/S0010-2180(97)00323-4

[18] Baillot, F., Bourehla, A., and Durox, D., "The Characteristics Method and Cusped Flame Fronts," *Combustion Science and Technology*, Vol. 112, 1996, pp. 327–350. doi:10.1080/00102209608951963

[19] Durox, D., Baillot, F., Searby, G., and Boyer, L., "On the Shape of Flames Under Strong Acoustic Forcing: A Mean Flow Controlled by an Oscillating Flow," *Journal of Fluid Mechanics*, Vol. 350, 1997, pp. 295–310. doi:10.1017/S0022112097006940

[20] Rajaram, R., and Lieuwen, T., "Parametric Studies of Acoustic Radiation from Premixed Flames," *Combustion Science and Technology*, Vol. 175, 2003, pp. 2269–2298. doi:10.1080/714923281

[21] Boyer, L., and Quinard, J., "On the Dynamics of Anchored Flames," *Combustion and Flame*, Vol. 82, No. 1, 1990, pp. 51–65. doi:10.1016/0010-2180(90)90077-5

[22] Clanet, C., Searby, G., and Clavin, P., "Primary Acoustic Instability of Flames Propagating in Tubes-Cases of Spray and Premixed Gas Combustion," *Journal of Fluid Mechanics*, Vol. 385, 1999, pp. 157–197. doi:10.1017/S0022112099004231

[23] Cho, J. H., and Lieuwen, T., "Laminar Premixed Flame Response to Equivalence Ratio Oscillations," *Combustion and Flame*, Vol. 140, No. 1, 2005, pp. 116–129. doi:10.1016/j.combustflame.2004.10.008

[24] McIntosh, A. C., "Deflagration Fronts and Compressibility," *Philosophical Transactions. Series A, Mathematical, Physical, and Engineering Sciences.*, Vol. 357, 1999, pp. 3523–3538. doi:10.1098/rsta.1999.0507

[25] Ducruix, S., Durox, D., and Candel, S., "Theoretical and Experimental Determinations of the Transfer Function of a Laminar Premixed Flame," *Proceedings of the Combustion Institute*, Vol. 28, 2000, pp. 765–773. doi:10.1016/S0082-0784(00)80279-9

[26] Baillot, F., Durox, D., and Prud'homme, R., "Experimental and Theoretical Study of a Premixed Vibrating Flame," *Combustion and Flame*, Vol. 88, No. 2, 1992, pp. 149–168. doi:10.1016/0010-2180(92)90049-U

[27] Matalon, M., and Matkowsky, B., "Flames as Gasdynamic Discontinuities," *Journal of Fluid Mechanics*, Vol. 124, 1982,

pp. 239–260.
doi:10.1017/S0022112082002481

[28] Schuller, T., DuCruix, S., Durox, D., and Candel, S., "Modeling Tools for the Prediction of Premixed Flame Transfer Functions," *Proceedings of the Combustion Institute*, Vol. 29, 2002, pp. 107–113.
doi:10.1016/S1540-7489(02)80018-9

[29] Durox, D., Schuller, T., and Candel, S., "Combustion Dynamics of Inverted Conical Flames," *Proceedings of the Combustion Institute*, Vol. 30, 2005, pp. 1717–1724.
doi:10.1016/j.proci.2004.08.067

[30] Wang, H., Law, C. K., and Lieuwen, T., "Linear Response of Stretch-Affected Premixed Flames to Flow Oscillations," *Combustion and Flame*, Vol. 156, No. 4, pp. 889–895.
doi:10.1016/j.combustflame.2009.01.012

[31] Preetham, Thumuluru, S. K., and Lieuwen, T., "Linear Response of Premixed Flames to Flow Oscillations: Unsteady Stretch Effects," AIAA Paper 2007-0176, 2007.

C. Avedisian
Associate Editor